university of groningen / faculty of mathematics and natural sciences

University of Groningen
Zernike Institute
for Advanced Materials

Pump-Probe measurements on the ferroelectric phase transition of the $CuCl_4(C_6H_5CH_2CH_2NH_3)_2$ organic-inorganic hybrid

Physics Bachelor Thesis

performed in the group of

Optical Condensed Matter Physics

Diederik Perdok[1]

Supervisors: Antonio Caretta[2] and Prof. Paul van Loosdrecht[3]

August 31, 2011

[1] D.W.Perdok@Student.Rug.nl
[2] A.Caretta@rug.nl
[3] P.H.M.van.Loosdrecht@rug.nl

Abstract

The ferroelectric phase transition at 340 K of the $CuCl_4(C_6H_5CH_2CH_2NH_3)_2$ organic-inorganic hybrid was investigated using the pump-probe method, using light polarisation rotation as a probe for ferroelectricity. Transmission and birefringence data were used to select the probe wavelength of 650 nm; the pump wavelength was 800 nm. We found that as a result of pump pulses exciting copper d-d transitions, the rotation exponentially decreased until the material reached a less birefringent state. The decay parameters (i.e. the time in which the rotation was reduced to e^{-1} of its original value) were (5.9 ± 0.2) ps at 291 K and (21.1 ± 0.4) ps at 329 K. The change in rotation was calculated to be the result of overall heating of the material. However, it was impossible to induce the phase transition by pumping, because the energy required turned out to be far above the damage threshold of the material. With the fluence equal to the damage threshold at 291 K and 1 kHz repetition rate, only 0.11 % of the copper ions were excited.

Contents

Chapter 1

Introduction

Hybrid organic-inorganic framework materials may be defined as 'compounds that contain both inorganic and organic moieties as integral parts of a network with infinite bonding connectivity in at least one direction' [1]. Combining organic and inorganic materials enables researchers to synthesize and characterize a vast range of new materials. Their diverse properties including (anti)ferromagnetism, ferrimagnetism, metamagnetism, ferroelectricity, multiferroicity (i.e. multiple ferroic orderings simultaneously), photo- and electoroluminescence, nonlinear optical activity, birefringence and semiconduction [1] have made them the subject of a lot of research during the past decades. Hybrid materials may find application in electronics [2], medicine [3, 4], and those of the porous kind in catalysis, gas storage, sorption, separations and sensors [1, 5].

Recently, research on the $CuCl_4(C_6H_5CH_2CH_2NH_3)_2$ hybrid has been done in our group by Davood Abbaszadeh and Antonio Caretta. The project described in this thesis focuses on the ferroelectricity of this material, by means of pump-probe measurements on the ferroelectric phase transition.

Chapter 2

Theory and Goal

The $CuCl_4(C_6H_5CH_2CH_2NH_3)_2$ hybrid has a structure consisting of inorganic sheets interleaved with two layers of organic molecules, as displayed in figure 2.1. The inorganic layers consist of $CuCl_6$ octahedra in a perovskite-like structure; the organic part consists of $C_6H_5CH_2CH_2NH_3^+$ molecules. Due to electrostatic attraction, the inorganic molecules point towards the octahedra with their NH_3 group. Using the classification system introduced by Cheetham et al. [1], this structure is classified as I^2O^0 [2].

The material undergoes a structural phase transition at 340 K where it becomes polar. The transition shows first-order character like latent heat and a ~ 5 K hysteresis (i.e. upon heating the transition occurs at ~ 345 K and upon cooling at ~ 335 K). However, the transition is only 'weakly first order' because of differences observed between heating and cooling the material which can be ascribed to fluctuations characteristic of weakly first order transitions [2]. Below the phase transition there is a distortion of the inorganic layers, as displayed in figure 2.1. As discussed by Arkenbout, the dielectric polarisation in this phase is explained by the ammonium groups being positioned off-centre from the surrounding Cu ions, generating a dipole. Since the NH_3 groups can assume two off-centred positions separated by a potential barrier, each causing a dipole moment in a different direction, a macroscopic polarisation can be maintained by cooling the material through the phase transition in an electric field. The definition of ferroelectricity strictly requires it to be possible to change the polarisation by applying an electric field (without causing breakdown of the crystal), for a material to be called ferroelectric as opposed to just polar [6]. Conclusive evidence for this material being ferroelectric or not still has to be found, however. Still, for convenience the material will be called ferroelectric in this thesis.

In both phases there is a large structural anisotropy: along the inorganic sheets the material looks very different than in the direction along the organic molecules. It is therefore not surprising that the material is (linearly) birefringent in both phases, which is the phenomenon that the propagation speed of linearly polarised light depends on its polarisation with respect to a crystal axis called the optical axis. The difference in speed between two waves linearly polarised parallel and perpendicular to the optical axis (called the extraordinary and ordinary waves respectively) causes a phase difference between them. The phenomenon is caused by a difference in dielectric constant along each axis and hence, by the well known equation $c = \sqrt{\epsilon_r \mu_r}$ for the speed of light, a difference in propagation speed and refractive index. Birefringent materials can be used to create

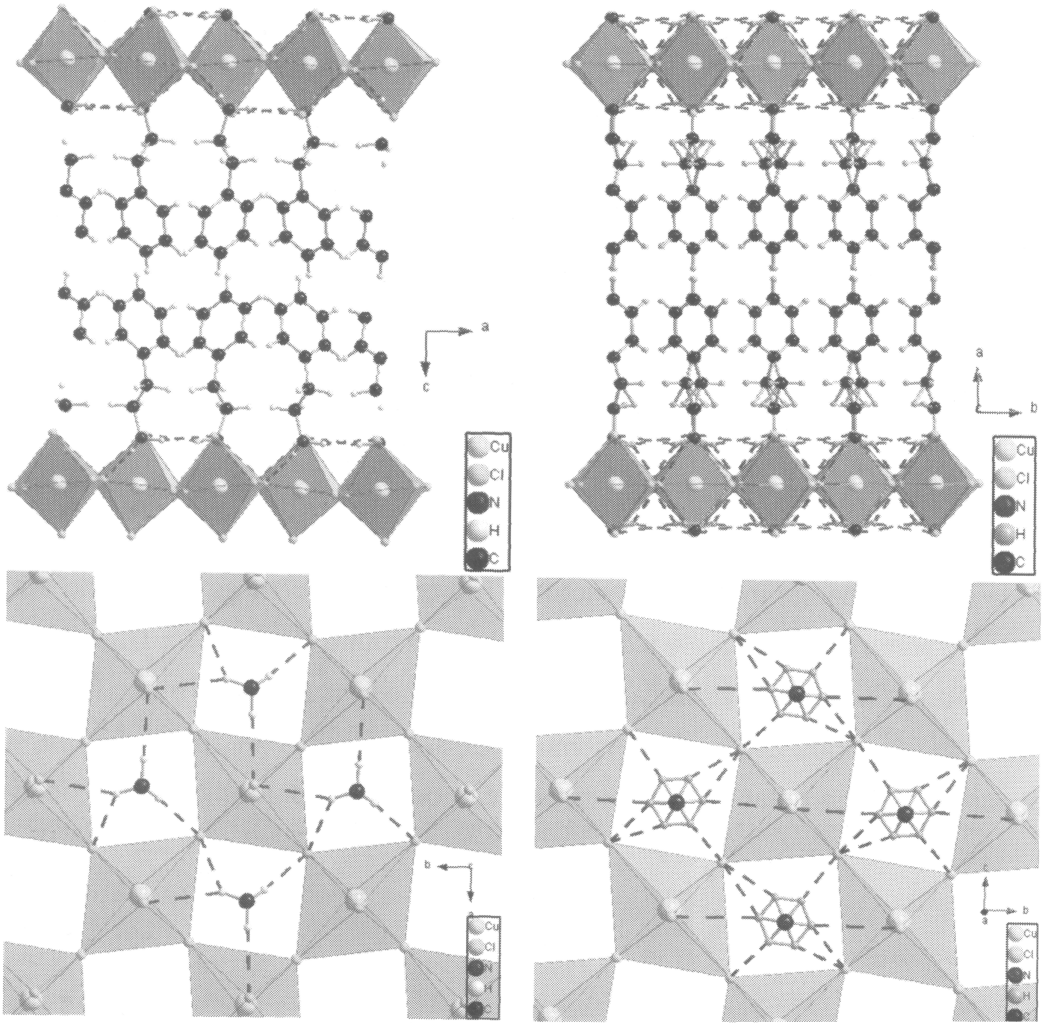

Figure 2.1: Crystal structure below (left) and above (right) the ferroelectric phase transition [2].

optical elements that manipulate the polarisation of light; for example by rotating it (a half-wave plate) or by changing it from linearly to circularly polarised and vice versa (a quarter wave plate) [7, 8]. The material also exhibits (linear) dichroism, which is another optical anisotropy resulting from structural anisotropy. In a dichroic material the absorption depends on the polarisation of light [9].

In our group, this material is being studied because of it's multiferroicity: below 340 K it's polar and possibly ferroelectric, and below 13 K it's ferromagnetic [2]. It would be interesting to see if ferromagnetism and ferroelectricity can somehow be coupled in hybrid materials. An application of this would be electrically controlled magnetic storage [2]. This project is part of the research into the cause of the ferroelectricity, and consists mainly of measurements on the ferroelectric phase transition using the pump-probe technique (to be explained further in section 3.3). To test the aforementioned hypothesis that a macroscopic polarisation is caused by ordering of the ammonium groups, the rotational mode of these groups should be excited whilst measuring the dielectric polarisation. This

can be done using a laser system producing $6250\,\mathrm{cm}^{-1}$ pump pulses (N-H bend mode [10]) and a way to probe this polarisation. Birefringence can be used as probe, because the dielectric constant along the direction of polarisation changes when the spontaneous polarisation disappears, which will then show up in the birefringence. Indeed, we know from earlier measurements by Abbaszadeh that the birefringence changes sharply at the ferroelectric phase transition (but doesn't disappear) [9]. Of course, after exciting the N-H bend mode the material will quickly relax, so the birefringence will quickly assume the value it had before excitation. Therefore we require a means to measure the birefringence as a function of time with high resolution, and a short, high power pump pulse to excite many NH_3 groups before the material has the chance to relax. This is exactly what can be achieved by using the pump-probe method.

Here, 800 nm will be used as pump wavelength and rotation of light (caused by the birefringence of the material) will be used as probe. The goal of this project is to get a good pump-probe signal showing signs of the ferroelectric phase transition, using 800 nm as pump wavelength and gather data that can be compared to the results obtained when pumping with $6250\,\mathrm{cm}^{-1}$ later (but not in this project).

Chapter 3

Experimental Setup

3.1 Absorption

To measure the absorbtion of the samples, the setup described in figure 3.1a was used. It consisted of a white light source followed by a monochromator, a chopper, the sample, a detector and a lock-in amplifier. A computer connected to the monochromator and the lock-in amplifier allowed the recording of the light intensity as a function of wavelength. The transmission of the sample was obtained by dividing a spectrum with the sample in place, by a reference spectrum taken without the sample. From the transmission (T) we calculated the absorption coefficient (α) using $\alpha = -\frac{\ln T}{d}$, where d is the thickness of the sample as measured using a micrometer.

3.2 Birefringence

A modified version of the setup described in section 3.1 was used by Davood Abbaszadeh to measure the birefringence by adding two polarisers, a PEM (PhotoElastic Modulator), and two lock-in amplifiers (figure 3.1b). With respect to the first polariser, the sample and the PEM were rotated by 45° and the second polariser by 90°. The PEM consists of a photoelastic material whose birefringence was modulated by piezoelectric transducers according to $\Delta_{PEM} = A\cos(\Omega t)$. Here Δ_{PEM} is the birefringence of the PEM (defined as the phase difference induced between the ordinary and extraordinary waves), $A = 2.405\,\text{rad}$ is the amplitude and $\Omega = 50\,\text{kHz}$. A calculation now shows that the resulting voltage measured by the detector contains a DC term and terms oscillating at Ω, 2Ω and higher frequencies [11]. The DC component of the voltage from the detector was measured by a lock-in using the reference signal from the chopper controller; the terms at Ω and 2Ω were measured by lock-ins using the signal from the PEM controller as reference. Finally, the birefringence of the sample, expressed as the phase difference induced between the ordinary and extraordinary rays, was given by $\Delta = \tan^{-1}(\frac{J_2(A)}{J_1(A)} \times \frac{V_\Omega}{V_{2\Omega}})$ (J_n is the n^{th} order Bessel function of the first kind)

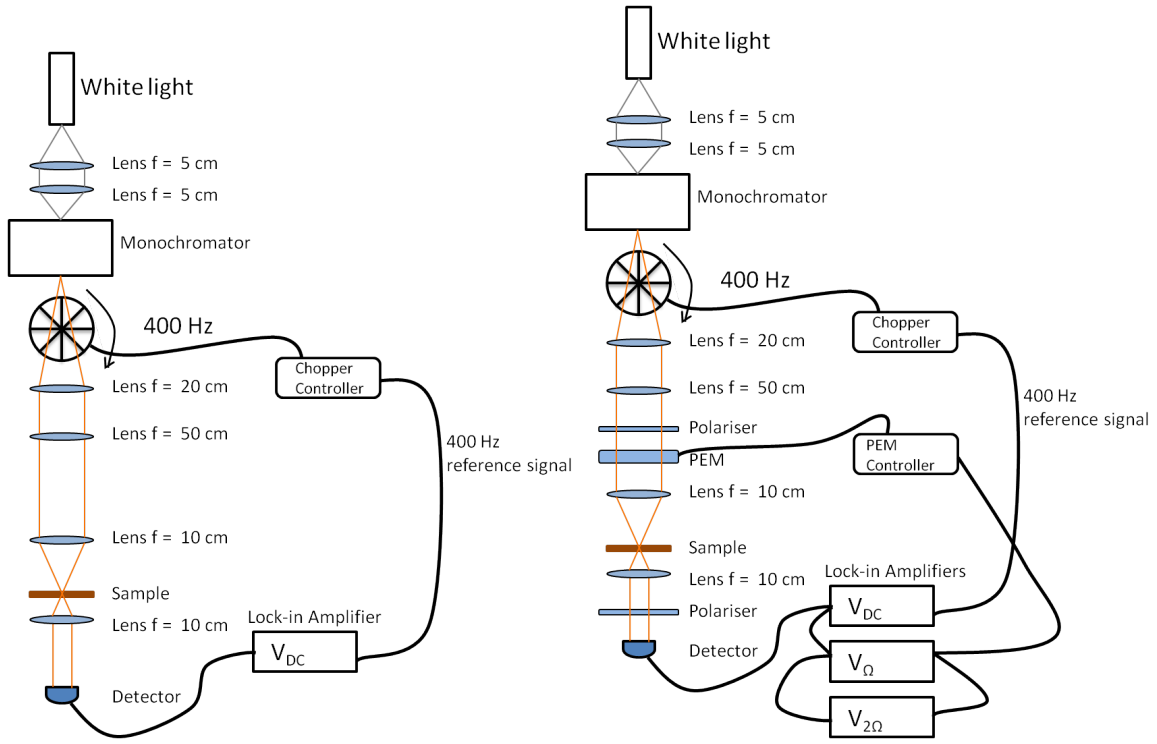

(a) Transmission setup (b) Birefringence setup

Figure 3.1: Schematic representations of the setups used to measure the transmission and birefringence

3.3 Pump-Probe

The Pump-Probe method is a method for doing time-resolved ultrafast spectroscopy. It works by exciting the sample under investigation by a 'pump' beam of high power ultrashort laser pulses (10^{-15} s – 10^{-13} s). A second beam of ultrashort pulses, called the 'probe' beam, goes through the same spot on the sample as the pump. The probe power is much lower as to not have an effect on the temperature of any degree of freedom of the sample. The effect of the pump on for example the absorption, reflection or rotation of the probe is measured as a function of time. This can be done by adjusting the time delay between the arrival of the pump and probe pulses on the sample by adjusting the path length of either beam by moving a delay line. In this way, ultrafast processes in a material can be followed with a time resolution comparable to the duration of the laser pulses [12].

Figure 3.2 shows a schematic of the pump-probe setup that we used to measure the rotation induced by the copper hybrid at 650 nm, and the change in the rotation as a result of 800 nm pump pulses. This was done to investigate the phase transition at 340K. A Ti:Sapphire laser produced an 800 nm pulsed beam with a repetition rate of 1000 Hz; the pulse energy could be set by using different attenuating filters. A beam splitter split it into two beams; one was used to pump the sample after going through a chopper that alternately blocked 3 pulses, and allowed through 3 pulses; the other was used to pump the TOPAS (Travelling wave Optical Parametric Amplifier of Superfluorescence;

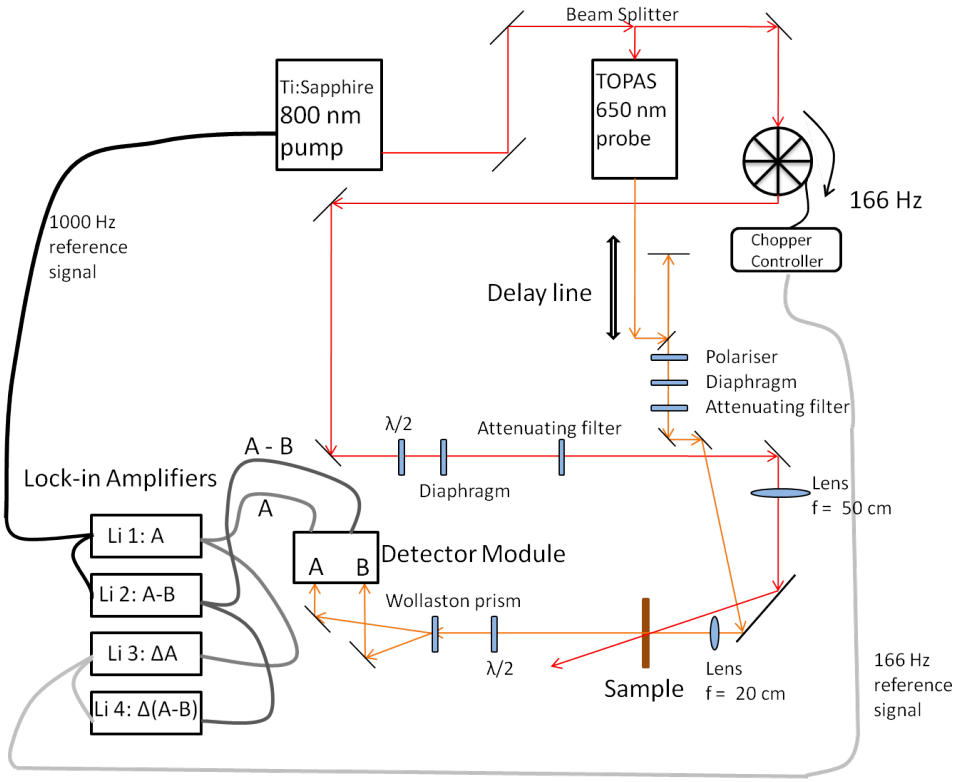

Figure 3.2: Schematic of the pump-probe setup

model TOPAS-800 by 'Light Conversion'). The output of the TOPAS (also at 1 kHz) was used as probe and set to 650 nm because at this wavelength the material exhibits high birefringence and transmission. A polariser was used to vertically polarise the probe; the polarisation of the pump could be varied using a half-wave plate. The path length of the probe could be varied by moving a retroreflector on a translation stage such that the time difference between the pump and the probe pulse on the sample was given by $\Delta t = 2\frac{d-d_0}{c}$ where d_0 is the zero-postion of the translation stage. The lengths of the pump and probe pulses resulted in a temporal resolution of ~ 100 fs.

The pump and probe beams were focussed on the same spot on the sample, the pump being slightly larger in diameter (0.12 mm as measured using a cutter) than the probe (0.10 mm). This ensured that only the pumped part of the sample was probed. The sample was located in a cryostat allowing for precise temperature control up to 329 K; the room temperature in the lab was kept at 18 °C. After going through the sample, the probe beam went through a Berek-compensator setup as a half-wave plate, followed by a Wollaston prism. This prism split the beam in its vertically and horizontally polarised components, which were detected by detectors A and B respectively. Both detectors were covered by a filter blocking any pump light that might otherwise be scattered onto them (but allowing through the 650 nm probe light). The quantities A and $A - B$ from the detector module were sent to a total of four lock-in amplifiers, after the $A - B$ signal had been preamplified by an amount variable between 2× and 400× (for every measurement the highest amplification that wouldn't overload the lock-ins was chosen).

The connections to the 4 lock-in amplifiers are shown in figure 3.2. The pulse repetition rate of the pump laser, and therefore also of the probe beam, was 1000 Hz; by using

this as a reference signal, the lock-ins 1 and 2 could measure the signals A and $A-B$. Because the pump beam was being chopped at 166 Hz, the change in A and $A-B$ as a result of the pump (called ΔA and $\Delta(A-B)$ from now on) could be measured by using the 166 Hz signal from the chopper controller as a reference signal for lock-ins 3 and 4. Finally, the values from the lock-in amplifiers were recorded by a computer as a function of the position of the delay line (i.e. as a function of time). Since the phase between the input signal and the reference signal can be freely set on a lock-in amplifier, care has to be taken when determining the signs of the output signals. To check the sign of A and $A-B$ it sufficed to block one of the detectors and observe the readings on lock-ins 1 and 2. To set the signs of the ΔA and $\Delta(A-B)$ signals, first one of the filters in front of the detectors was removed; the phase was now set to get a positive signal from the scattered pump light.

As shown in appendix A, the rotation of light by the sample (θ) and the change in it as a result of the pump ($\Delta\theta$), can be calculated as follows:

$$\theta = \frac{1}{2}\cos^{-1}\left(\frac{A-B}{2A-(A-B)}\right) \tag{3.1}$$

After measuring θ the Berek-compensator was rotated to make $A-B \approx 0$. Now $\Delta\theta$ is

$$\Delta\theta \approx \frac{(A-B)\,\Delta A - A\,\Delta(A-B)}{(2A-(A-B))^2} \tag{3.2}$$

From the Jones calculus in appendix B it follows that $\Delta\theta$ varies linearly with the change in the birefringence.

Chapter 4

Results

4.1 Data

4.1.1 Transmission, Absorption and Reflectivity

Figure 4.1 shows the transmission of 8 different samples between 350 nm and 1000 nm at 18 °C (samples A, and E were measured by Davood Abbaszadeh). The two measurements of sample 1 were made on different spots on the sample; the differences in the spectra suggest the sample thickness wasn't uniform. Table 4.1 lists the sample thicknesses measured with a micrometer. Comparing this with the graphs, we see that the transmission at 780 nm could be used to estimate the sample thickness, unlike the transmission at 600 nm which appears to be thickness independent. This is explained by the fact that the absorption is so low at the latter wavelength, that reflection dominates, which is thickness independent.

Of special interest is the transmission at 800 nm and 650 nm, because these will be used as pump and probe wavelengths respectively. We see that the transmission at 800 nm is very low, ensuring (nearly) all energy in the pump pulses will be absorbed; the cause of the absorption band around 800 nm is Cu^{2+} d-d transitions [13]. At 650 nm the transmission is fairly high so there will be no problems detecting the probe light when doing the pump-probe measurements.

Plots of the absorption coefficient ($\alpha = -\frac{\ln T}{d}$ where T is transmission and d is thickness) are shown in figure 4.2 for all 8 samples. The region below 500 nm is not plotted

sample	thickness (mm)
1	0.104
2	0.058
3	0.165
4	0.173
5	0.163
A	0.052
C	0.046
E	0.111

Table 4.1: Sample thickness

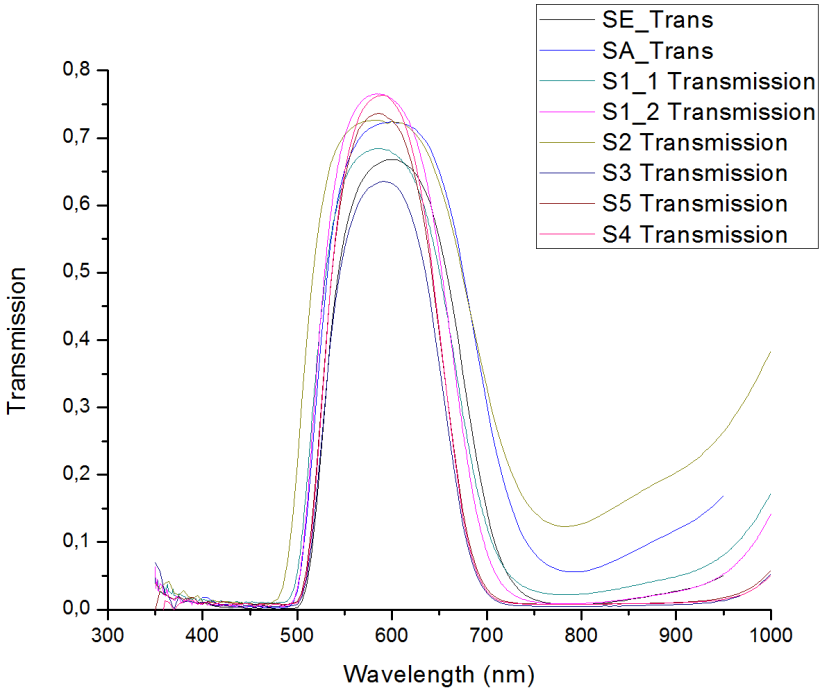

Figure 4.1: Transmission

because due the transmission being comparable to the noise level there, the obtained absorbtion data is not reliable (the same goes for certain samples in the 750 nm – 900 nm region). We see that at 800 nm $\alpha \approx 50\,\mathrm{mm}^{-1}$, meaning that in the pump-probe measurements, 80% of the pump pulse energy will be absorbed in the first $\sim 32\,\mu\mathrm{m}$ of the sample. So most of the pump-probe signal will be from a small part of the sample; the rest of it will not contribute much due to its low excitation.

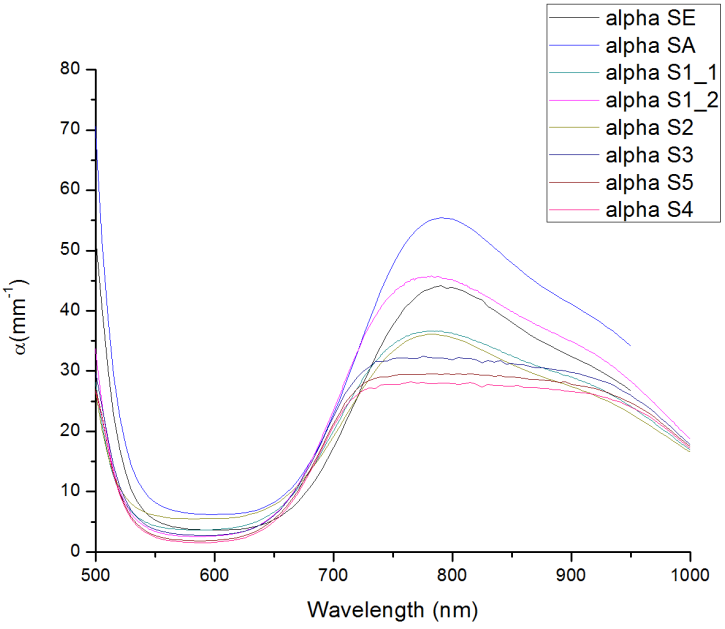

Figure 4.2: α vs. wavelength

There are large differences between the graphs in figure 4.2, caused by neglecting reflection when calculating α (and perhaps in part caused by differences in the concentration of impurities and lattice defects). To improve the absorption data, it was attempted to extract the absorption coefficient and the reflectivity from the data by globally fitting the equation $T = (1-R)^2 \sum_{n=0}^{\infty} e^{-\alpha d(1+2n)} R^{2n}$ to the transmission data. The results were obtained from the five measurements with the highest transmission, because this gave the lowest uncertainty. Figure 4.3 shows the results including 95% confidence intervals. The uncertainty in the results is very large; it might be better to try and measure the reflectivity directly, and use that to deduce the absorption from the transmission data. Another way to improve the results would be to use a fitting algorithm that allows the use of constraints (i.e. $0 \leq R \leq 1$ and $\alpha \geq 0$).

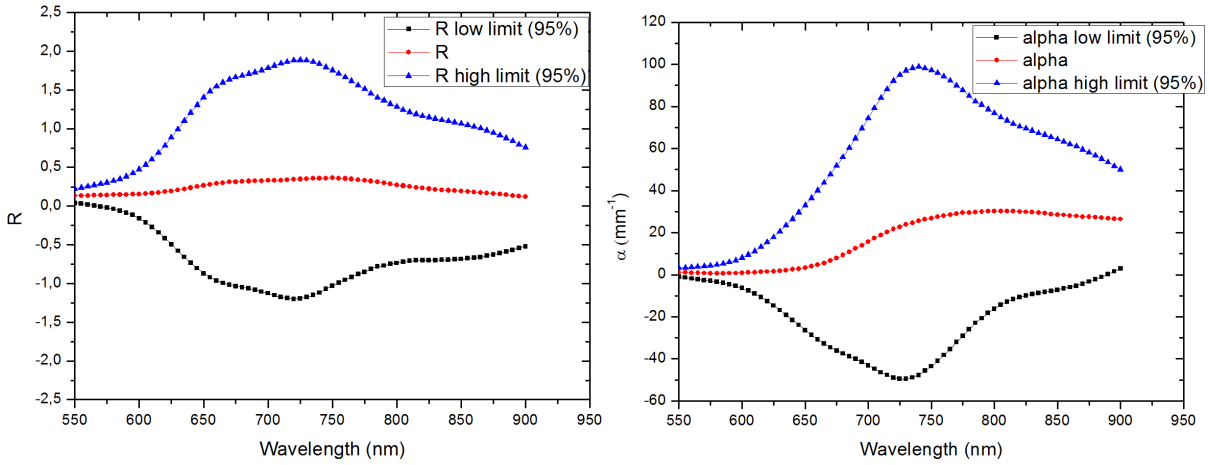

(a) Reflectivity (b) Absorption coefficient α

Figure 4.3: Results of globally fitting the transmission data

4.1.2 Birefringence

Davood Abbaszadeh investigated the birefringence of our copper hybrids [9]. This is relevant for our purpose because we use rotation of light to probe the phase transition around 340K. Figure 4.4 shows the birefringence expressed as the difference in refractive index between the ordinary and the extraordinary axes (Δn) as function of wavelength and temperature. We chose 650 nm as probe wavelength because at this wavelength both the birefringence and the transmission are high. Since we want to investigate the phase transition around 340K, it is useful to look at the birefringence around this temperature at various wavelengths; this is displayed in figure 4.5.

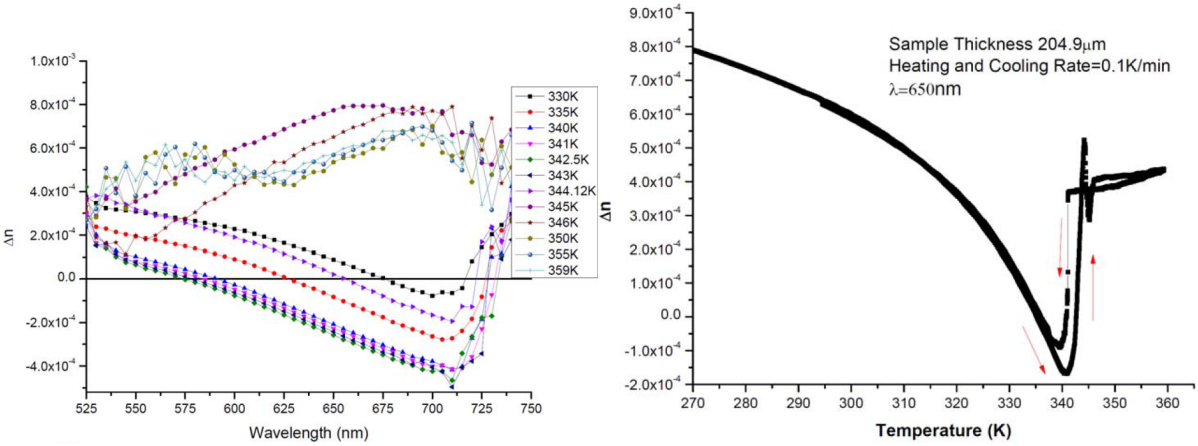

(a) Birefringence at different temperatures (b) Birefringence at 650 nm as function of T

Figure 4.4: Birefringence of $CuCl_4(C_6H_5CH_2CH_2NH_3)_2$

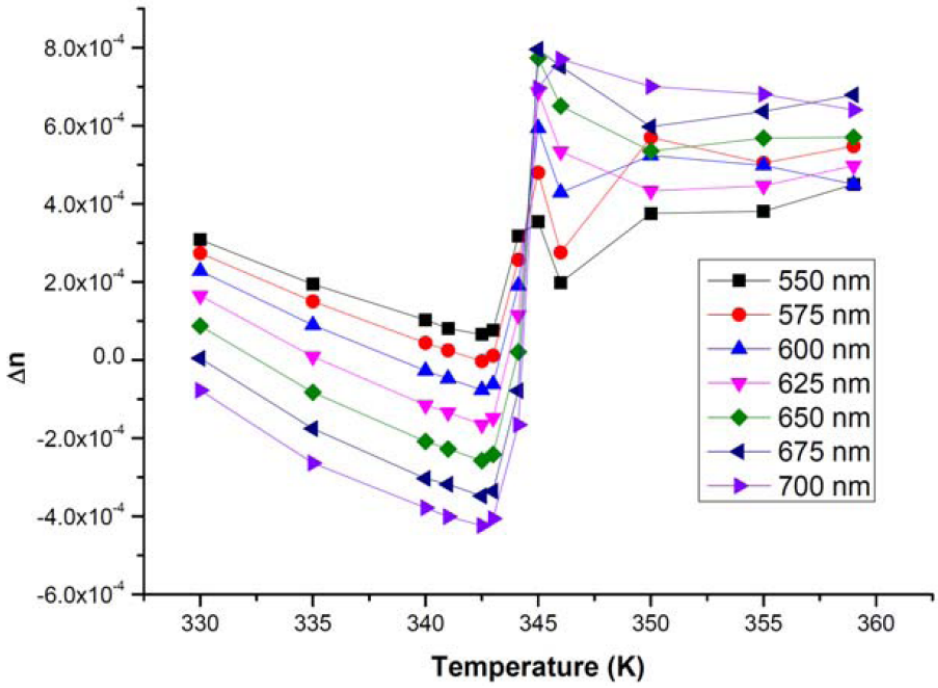

Figure 4.5: Birefringence around the ferroelectric phase transition

The data shows that if enough energy is pumped into the sample to reach the phase transition, a clear change in the birefringence will result when doing the pump-probe measurements. Therefore the rotation of 650 nm light is a suitable probe for the ferroelectric phase transition.

4.1.3 Pump-Probe

Pump-probe measurements were done at room temperature (18 °C) and at 329 K, all on the same sample, having a thickness of (76 ± 7) µm as determined from its transmission.

The results are shown in figure 4.6. Intuitively one would expect all the graphs to

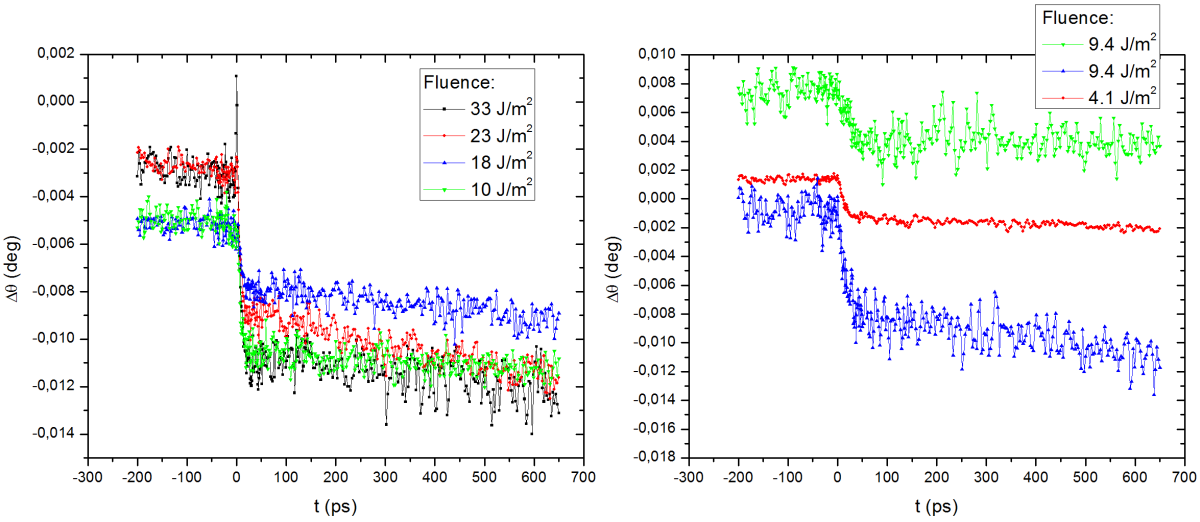

(a) Room temperature and ambient pressure (b) 329 K and 100 mbar

Figure 4.6: Pump-induced change in probe-light rotation as function of time

be at $\Delta\theta = 0$ before $t = 0$, since the pump pulse arrives at $t = 0$. But as can be seen from the graphs, only 1 of the transients is, and the others are shifted vertically. This might be caused by 800 nm light being scattered into the detectors (although there was an 800 nm blocking filter immediately in front of them). A measurement with the pump beam blocked could confirm this. It might also be caused by the previous pulse exciting a long-lived state, but this doesn't explain why the effect differs so much across different measurements. In any case it is useful to view the graphs after they have been horizontally shifted to start at the same level, as in figure 4.7.

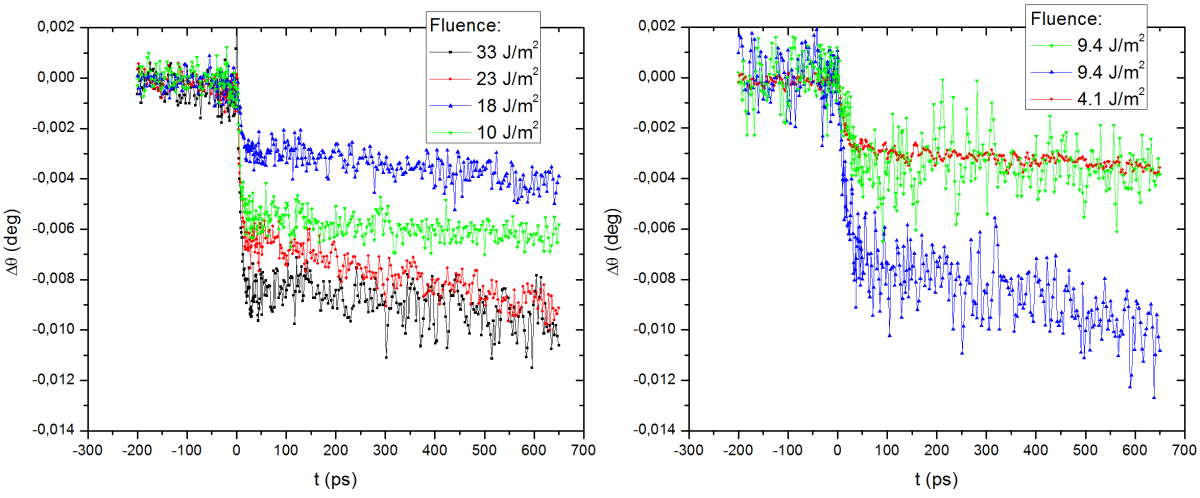

(a) Room temperature and ambient pressure (b) 329 K and 100 mbar

Figure 4.7: Same as figure 4.6, but all the graphs shifted to start at $\Delta\theta = 0$

The change in transmission (if any) was smaller than the noise level, so no $\frac{dT}{T}$ data

was obtained.

4.2 Analysis

4.2.1 Relaxation time

Looking at the pump-probe results in figure 4.7 in more detail, a peak can be seen at the arrival of the pump pulse at $t = 0$ in the measurement with the highest power. This is most likely due to the optical Kerr-effect and/or Pockels-effect, which is a change in the refractive index induced by the electric field of the light itself [12]. A detailed view is in figure 4.8. Then we see that in the first 20 fs after the arrival of the pulse $\Delta\theta$ becomes negative (its absolute value looks to be independent of power; this is only because the measurements were done on different parts of the sample however; also see section 4.2.2). Since θ itself was measured to be positive, a negative $\Delta\theta$ means a reduction of rotation. A reduced rotation was indeed expected because figure 4.4b shows a decrease in birefringence with an increase in temperature. Also, a solid-state system generally becomes less ordered upon heating, and a lower order (less anisotropy) means lower birefringence which in turn implies less rotation. However, the birefringence (figs. 4.4 and 4.5) shows a sharp increase when heating past the phase transition. Not observing this is the first indication that the samples were not pumped up to the phase transition; more about this in section 4.2.2. After this initial drop, $\Delta\theta$ stays pretty much constant: apparently the material quickly relaxes to a more long-lived state after Cu^{2+} d-d transitions have been excited by the pump pulse. Our delay line did not allow a long enough time span to observe the sample recovering to its initial state, so we only learned that the lifetime of this state is at least 650 ps.

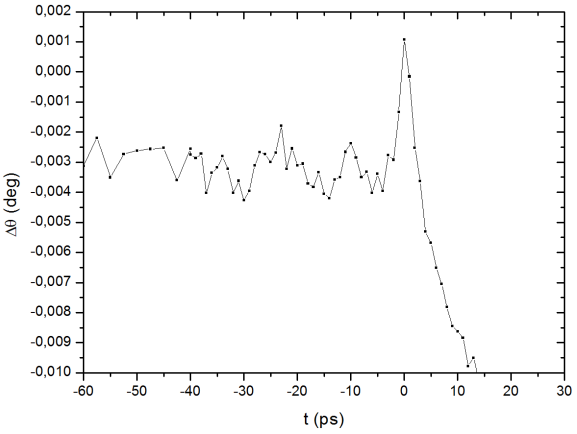

Figure 4.8: Zoomed in view of the peak at $t = 0$ in the 33 J m^{-2} measurement

The time it takes the sample to relax to this less birefringent and longer-lived state is characterised by the time in which $\Delta\theta$ drops. By measuring this relaxation time as a function of pump wavelength, i.e. as a function of the part of the molecules that's pumped, insight could be gained into which parts of the molecule are directly responsible for the ferroelectricity. For example, when pumping a functional group that plays an important role in the ferroelectricity, a relatively fast reduction in rotation is expected.

To determine the relaxation time from the pump-probe data, the decaying part of each curve was fitted to $\Delta\theta = \theta_0 + Ae^{-\frac{t}{t_r}}$. An example is displayed in figure 4.9. The resulting values for the parameter t_r are in table 4.2. These data clearly show a higher t_r at the higher temperature; it would require more measurements to say anything about the energy dependence. The average t_r values, using the inverse square errors as weights, are $t_r = (5.9 \pm 0.2)$ ps at room temperature and $t_r = (21.1 \pm 0.4)$ ps at 329 K (the error in the averages is $w^{-1/2}$; w is the sum of the weights [14]). Apparently, when going closer

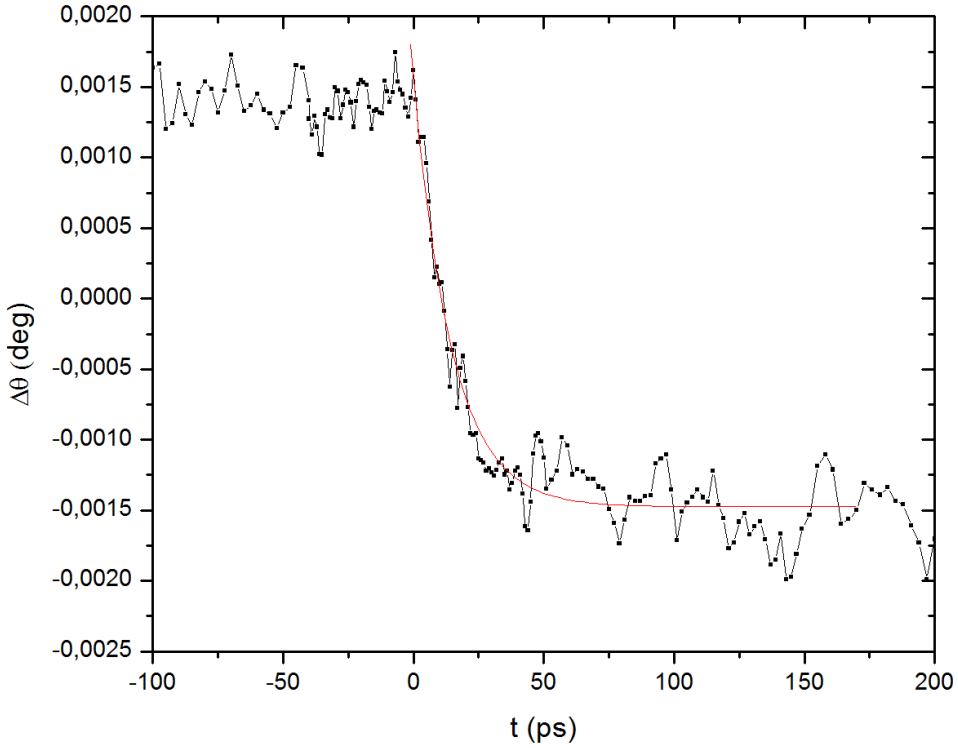

Figure 4.9: Fitting an exponential decay to the 4.1 J m^{-2} pump-probe measurement

to the phase transition, it takes more time for energy to dissipate from the Cu ions to the ammonium groups. To understand this strong temperature dependence of t_r, we may look at figure 4.4b: closer to the phase transition, the birefringence is lower and more strongly temperature dependent. Having a lower birefringence could mean that more ammonium groups are in an excited state, leaving less groups available to be excited. This might explain why the relaxation time is longer at 329 K than at 291 K, since the only way for excess energy in the inorganic layers to reach the organic parts would be through the ammonium groups.

Fluence J m^{-2}	Temperature K	t_r ps	θ_0 deg $\times 10^{-3}$	A $\times 10^{-3}$
33	291	5.4 ± 0.4	-11.08 ± 0.05	12.6 ± 0.6
23	291	6.0 ± 0.4	-9.15 ± 0.05	8.4 ± 0.4
18	291	7 ± 1	-8.00 ± 0.04	4.1 ± 0.6
10	291	6.4 ± 0.6	-10.64 ± 0.04	6.9 ± 0.4
9.4	329	19 ± 2	-8.6 ± 0.1	7.2 ± 0.3
9.4	329	22.8 ± 0.4	3.7 ± 0.2	4.1 ± 0.4
4.1	329	14.5 ± 0.8	-1.40 ± 0.03	3.06 ± 0.09

Table 4.2: Relaxation time

4.2.2 Power dependence

To analyse how $\Delta\theta$ depends on the pump power, measurements have been made at 25 ps all on the same spot on the sample. Figure 4.10 displays the results. If the absorbed

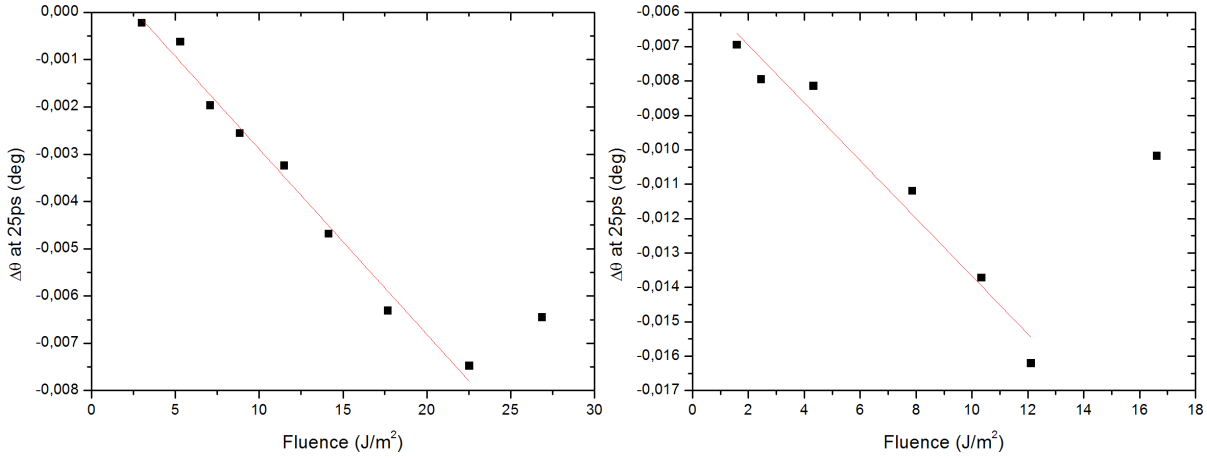

(a) Room temperature (291 K) and ambient pressure

(b) 329 K and 100 mbar

Figure 4.10: Induced rotation change as function of pump pulse energy

energy is high enough to increase the temperature past the phase transition, a change in the slope and/or shape of the graphs is to be expected as mentioned in section 4.1.2 in the discussion of figure 4.5. But, even close to the phase transition at 329 K, the behaviour is linear. The apparent deviation from linearity at high pulse energy is a result of burning the sample, not of probing the phase transition. This is confirmed by the fact that when going back to lower pulse energy, a much lower $\Delta\theta$ is measured than before, and by opaque black areas visible when observing the samples through a microscope. The black matter is probably carbon, suggesting its the organic part that gets damaged. The slopes of the lines fitted to figure 4.10 are $(-3.9 \pm 0.2) \times 10^{-4}$ deg J^{-1} m^2 at room temperature and $(-8.4 \pm 0.8) \times 10^{-4}$ deg J^{-1} m^2 at 329 K, but these values might vary across the surface of a sample. The fact that the slope of $\Delta\theta$ vs. fluence increases when going closer to the phase transition is consistent with the increasing negative slope of Δn vs. temperature in figure 4.4b. The damage threshold at 1 kHz seems to be ~ 21 J m^{-2} at 291 K and ~ 12 J m^{-2} at 329 K. Even when the fluence is equal to the damage threshold, the sample is not excited much, as the following calculation shows. From section 4.1.1 we know that 80% of the pulse energy is absorbed in the first 32 µm. An amount of energy of 0.8×240 nJ, which is the damage threshold at 291 K, can excite 7.7×10^{11} Cu^{2+} ions, which is only 0.11% of the Cu^{2+} in a cylinder of 32 µm length and 0.12 mm diameter (the laser spot size on the sample) [2]. A 150 nJ pulse, which is the damage threshold at 329 K, excites 0.06% of the copper.

The reason for not being able to see the phase transition is this low damage threshold. The specific heat of this Cu-hybrid is approximately 12 J K^{-1} g^{-1} around room temperature up to the phase transition [2]. Furthermore, from the volume and contents of the unit cell [2], the density can be calculated to be 1.49×10^3 kg m^{-3}. From these quantities we can now approximate the temperature increase to be as little as 30 mK, by taking a pulse energy of 240 nJ, and assuming 80% of the energy is absorbed in a volume of the focus

spot area (0.12 mm diameter) times 32 µm. From the slope of the graph in figure 4.4b at 291 K, we can estimate the change in Δn as result of this heating: $\Delta(\Delta n) \simeq -2.0 \times 10^{-7}$. It's useful to estimate $\Delta(\Delta n)$ from $\Delta\theta$ and compare it to this value. If it's the same order of magnitude, the change in Δn is probably just the result of heating the whole sample; if it's appreciably larger however, that means the copper ions have a direct effect on the birefringence.

We shall use equation B.9 to calculate the change in the $\Delta\phi$ from the measured value of $\Delta\theta$, and convert this to $\Delta(\Delta n)$:

$$\Delta\theta = \frac{4ab\Delta\phi\cos(4\beta)\sin\phi}{a^2 + b^2}$$

For that, we require the values of $\cos\beta$, $\sin\phi$ and a and b. The only information we have about β (the angle of rotation of the half-wave plate) is that it was set such that $A = B$. We don't know the values of a and b, so it's impossible to calculate β from the equations in appendix B, but since we are only interested in the order of magnitude of $\Delta(\Delta n)$ we shall assume $\cos 4\beta \approx 0.5$. We shall further make the approximation that $a = b$. From the results in section 4.1.2 we know that $\Delta n \approx 5.0 \times 10^{-4}$ at 650 nm in the temperature range were we did our measurements. Using the equation $\phi = \frac{2\pi d\Delta n}{\lambda_0}$ [9], where $\lambda_0 = 650$ nm (the wavelength in vacuum) and $d = (76 \pm 7)$ µm (sample thickness) we find $\sin\phi = 0.36$. Now we have

$$\Delta\theta = 0.36\Delta\phi$$

Taking $\Delta\theta = -0.007$ deg $= -1.2 \times 10^{-4}$ rad from our measurements, we find $\Delta\phi = -3.4 \times 10^{-4}$ rad. Again using $\phi = \frac{2\pi d\Delta n}{\lambda_0}$, the end result is $\Delta(\Delta n) = -4.6 \times 10^{-7}$.

Since this has the same order of magnitude as what was estimated to be the result of the temperature increase of the sample, we may conclude that the change in rotation that's observed is just the result of overall heating of the sample by the pump pulses.

Chapter 5

Conclusions and Discussion

The ferroelectric phase transition of the $CuCl_4(C_6H_5CH_2CH_2NH_3)_2$ organic-inorganic hybrid was investigated using the pump-probe method, using rotation of light as a probe for ferroelectricity. It was found that as a result of pump pulses exciting copper d-d transitions, the rotation decreased exponentially according to $\Delta\theta = \theta_0 + Ae^{-\frac{t}{t_r}}$. The decay parameters were $t_r = (5.9 \pm 0.2)$ ps at 291 K and $t_r = (21.1 \pm 0.4)$ ps at 329 K. It was argued that this difference was caused by more NH_3 groups already being excited at 329 K, making it harder for pump energy in the inorganic layers to reach the organic part of the material. Nothing could be concluded about the ferroelectric phase transition because the low damage threshold of the material ($21\,\mathrm{J\,m^{-2}}$ at 291 K and $12\,\mathrm{J\,m^{-2}}$ at 329 K) did not allow enough energy to be absorbed for the material to undergo the phase transition. Temperatures even closer to the phase transition should be used to more easily reach the phase transition, but our temperature control system did not allow this. At the damage threshold, the temperature increase as result of the energy in a pump pulse was calculated to be 30 mK, using the heat capacity. From birefringence vs. temperature measurements the change in the birefringence as result of this temperature increase was calculated to be $\Delta(\Delta n) \simeq -2.0 \times 10^{-7}$. From the observed change in rotation the change in the birefringence was calculated to be $\Delta(\Delta n) = -4.6 \times 10^{-7}$. Since these values differ by only a factor of 2, we concluded that the change in rotation was the result of overall heating of the sample.

However, the specific heat used to calculate the value of 30 mK was $12\,\mathrm{J\,g^{-1}\,K^{-1}}$, which is unusually high, and might be incorrect. It was calculated from heat flow measurements by Arkenbout [2]; the specific heat should be measured again to check this value. Still, even when using the more realistic value of $2\,\mathrm{J\,g^{-1}\,K^{-1}}$, the temperature increase would be 180 mK, and $\Delta(\Delta n) \simeq -12.0 \times 10^{-7}$. Since this is still the same order of magnitude as $\Delta(\Delta n) \simeq -4.6 \times 10^{-7}$, the conclusion remains the same.

In future experiments, the NH_3 groups could be pumped (~ 1580 nm) to test the hypothesis that the orientation of the NH_3 between the $CuCl_4$ octahedra causes the material to be polar. If this hypothesis is true, and if the damage threshold at this wavelength allows it, the phase transition should be observed in the macroscopic dipole moment at much lower power than the power required to simply heat the entire sample past the transition. Also, a lower relaxation time is to be expected because the relaxation path for the pump energy to reach the NH_3 rotational mode is shorter.

Acknowledgements

There is a lot of people without whom I couldn't have done this project, and I would like to thank all of them. First of all I would like to thank prof. Paul van Loosdrecht for allowing me to do this research in his group, for the idea of this project, for our discussions on how to interpret and process the results, and for reviewing the first version of this thesis. I would also like to thank Toni, for the day to day supervision and general help, for getting me started with the literature, for helping me with the experimental setup, for patiently explaining me the function of all the parts and how to use them, for helping me do the measurements, and for reviewing the first version. I should also thank Davood for showing me how to use the absorption setup. Furthermore, I am grateful to Ben, our newly assigned official 'Laser Safety Officer', for helping me not have any accidents. Then there were also Matteo, whom I thank for helping me on a few occasions, Foppe, whom I thank for helping me with 'global fitting', and Sven who deserves to be thanked for giving advice on how to improve the first version of this thesis. I would also like to thank the group of Solid State Materials for Electronics for producing the samples I used. And finally, I would like to thank everyone in the group of Optical Condensed Matter Physics for the many (birthday) cakes and the friendly atmosphere during the coffee and lunch breaks.

Bibliography

[1] A.K. Rao, C.N.R. an Cheetham and A. Thirumurugan. Hybrid inorganic-organic materials: a new family in condensed matter physics. *J. Phys.: Condens. matter*, 20(8), 2008.

[2] Anne Arkenbout. *Organic-Inorganic Hybrids: A Route towards Soluble Magnetic Electronics*. PhD thesis, Zernike Institute for Advanced Materials—University of Groningen, 2010.

[3] Maria Vallet-Regi, Montserrat Colilla, and Blanca González. Medical applications of organic-inorganic hybrid materials within the field of silica-based bioceramics. *Chem. Soc. Rev.*, 40(2), 2011.

[4] Alexandre Léonard, Philippe Dandoy, Emeric Danloy, Grégory Leroux, Christophe F. Meunier, Joanna C. Rooke, and Bao-Lian Su. Whole-cell base hybrid materials for green energy production, environmental remediation and smart cell-therapy. *Chem. Soc. Rev.*, 40(2), 2011.

[5] Clément Sanchez, Kenneth J. Shea, and Susumu Kitagawa. Recent progress in hybrid materials science. *Chem. Soc. Rev.*, 40(2), 2011.

[6] Charles Kittel. *Introduction to Solid State Physics*. John Wiley & Sons Inc, eighth edition, 2005.

[7] Mark Fox. *Optical Properties of Solids*. Oxford University Press, 2001.

[8] Paul van Loosdrecht and Maxim Pchenitchnikov. Photons and matter. Lecture slides.

[9] Davood Abbaszadeh. unpublished early version of master thesis.

[10] G Verkerk, J.B. Broens, R.E.A. Bouwens, P.A.M. de Groot, W. Kranendonk, M.J. Vogelezang, J.J. Westra, and I.M. Wevers-Prijs. 39—spectrometrie. In *BINAS*. Wolters-Noordhoff, Groningen, fifth edition, 2004.

[11] Hinds Instruments inc. *PEM manual: Appendix A*, 1996.

[12] Nikolai V. Tkachenko. *Optical Spectroscopy: Methods and Instrumentations*. Elsevier, 2006.

[13] G. Heygster and W. Kleemann. Optical investigations on magnetic and structural phase transitions of $(CH_3NH_3)_2CuCl_4$ and $(C_2H_5NH_3)_2CuCl_4$. *Physica B*, 89:165–176, 1977.

[14] H.J.C. Berendsen. *Goed meten met fouten.* Bibliotheek der RU Groningen, 2006.

[15] Prasanna S. Ghalsasi and Katsuya Inoue. Distorted perovskite structured organic-inorganic hybrid compounds for possible multiferroic behavior: $[n-alkyl]_2FeCl_4$. *Polyhedron*, 28, 2009.

[16] I. Pabst, Karolyi J., H. Fuess, and M. Couzi. Phase sequency of $[CH_3NH_3]_2CuClu_4$ studied by x-ray diffraction and low-frequency raman scattering. *Phys. Status Solidi A*, 155, 1996.

Appendix A

Calculating θ and $\Delta\theta$

Figure A.1 shows how the light polarisation angle θ is defined with respect to the vertical and horizontal components (detected by detectors A and B respectively). Since the probe light is vertically polarised, $\theta = 0$ when there's no rotation.

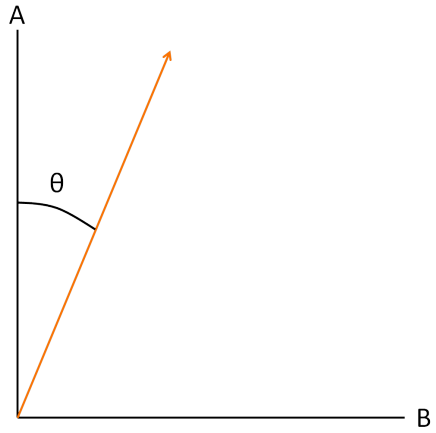

Figure A.1: Definition of the polarisation angle

The intensities measured by detectors A and B are given by

$$\begin{aligned} A &= E^2 \cos^2\theta \\ B &= E^2 \sin^2\theta \end{aligned} \tag{A.1}$$

Therefore,

$$\frac{A-B}{A+B} = \cos^2\theta - \sin^2\theta = 2\cos^2\theta - 1 = \cos 2\theta \tag{A.2}$$

$$\Rightarrow \theta = \frac{1}{2}\cos^{-1}\left(\frac{A-B}{A+B}\right) \tag{A.3}$$

When $A - B \simeq 0$ we can make a first order Taylor approximation of θ around $\pi/4$:

$$\frac{A-B}{A+B} = \cos 2\theta \simeq -2\left(\theta - \frac{\pi}{4}\right) \tag{A.4}$$

$$\Rightarrow \theta \simeq \frac{B-A}{2(A+B)} + \frac{\pi}{4} \equiv \frac{-x}{2(2A-x)} + \frac{\pi}{4} \tag{A.5}$$

where $x := A - B$. Now the differential is

$$\begin{aligned} d\theta &= \frac{\partial \theta}{\partial A}\, dA + \frac{\partial \theta}{\partial x}\, dx \\ &= \frac{x\, dA - A\, dx}{(2A - x)^2} \end{aligned} \tag{A.6}$$

By assuming dA and dx are sufficiently small, we can now approximate $\Delta\theta$ as

$$\begin{aligned} \Delta\theta &= \frac{x\, \Delta A - A\, \Delta x}{(2A - x)^2} \\ &= \frac{(A - B)\, \Delta A - A\, \Delta(A - B)}{(2A - (A - B))^2} \end{aligned} \tag{A.7}$$

Appendix B

Jones calculus of the pump-probe setup

Here we will do the Jones calculus of the probe part of the pump-probe setup described in section 3.3, to find out how a change in the birefringence of a sample affects the signals measured by detectors A and B.

We will describe our material, being birefringent and dichroic, as having two axes with different absorption and a phase difference induced between waves polarised along them:

$$\text{sample matrix} = \begin{pmatrix} ae^{i\phi} & 0 \\ 0 & b \end{pmatrix} \tag{B.1}$$

Here a and b describe absorption by the two axes, and ϕ is the birefringence expressed as the phase difference between the ordinary and extraordinary waves. During the measurements the sample was oriented to have maximum light rotation, which means the sample was rotated by $\frac{\pi}{4}$ radians:

$$\begin{aligned} \text{sample matrix} &= \begin{pmatrix} \cos\frac{\pi}{4} & \sin\frac{\pi}{4} \\ -\sin\frac{\pi}{4} & \cos\frac{\pi}{4} \end{pmatrix} \begin{pmatrix} ae^{i\phi} & 0 \\ 0 & b \end{pmatrix} \begin{pmatrix} \cos\frac{\pi}{4} & -\sin\frac{\pi}{4} \\ \sin\frac{\pi}{4} & \cos\frac{\pi}{4} \end{pmatrix} \\ &= \frac{1}{2} \begin{pmatrix} b + ae^{i\phi} & b - ae^{i\phi} \\ b - ae^{i\phi} & b + ae^{i\phi} \end{pmatrix} \end{aligned} \tag{B.2}$$

The light from the TOPAS had vertical polarisation before it passed through the sample, the half-wave plate (Berek compensator) the Wollaston prism and finally hit the detectors. Therefore the polarisation of the light that arrived at the Wollaston prism is described by:

$$\begin{aligned} &\text{half-wave plate matrix} * \text{sample matrix} * \text{vertically polarised light vector} \\ &= \begin{pmatrix} \cos 2\beta & \sin 2\beta \\ \sin 2\beta & -\cos 2\beta \end{pmatrix} \frac{1}{2} \begin{pmatrix} b + ae^{i\phi} & b - ae^{i\phi} \\ b - ae^{i\phi} & b + ae^{i\phi} \end{pmatrix} \begin{pmatrix} 0 \\ 1 \end{pmatrix} \\ &= \frac{1}{2} \begin{pmatrix} (b - ae^{i\phi})\cos 2\beta + (b + ae^{i\phi})\sin 2\beta \\ b(\sin 2\beta - \cos 2\beta) - ae^{i\phi}(\cos 2\beta + \sin 2\beta) \end{pmatrix} \end{aligned} \tag{B.3}$$

Here β is the angle over which the half-wave plate was rotated. The moduli of these

complex numbers are proportional to the intensities detected by detectors A and B:

$$\begin{aligned} B &= \frac{1}{2}((b - ae^{i\phi})\cos 2\beta + (b + ae^{i\phi})\sin 2\beta) * \frac{1}{2}((b - ae^{-i\phi})\cos 2\beta + (b + ae^{-i\phi})\sin 2\beta) \\ &= \frac{1}{4}(a^2 + b^2 - 2ab\cos 4\beta\cos\phi - (a^2 - b^2)\sin 4\beta) \end{aligned} \tag{B.4}$$

$$\begin{aligned} A &= \frac{1}{2}(b(\sin 2\beta - \cos 2\beta) - ae^{i\phi}(\cos 2\beta + \sin 2\beta)) * \frac{1}{2}(b(\sin 2\beta - \cos 2\beta) - ae^{-i\phi}(\cos 2\beta + \sin 2\beta)) \\ &= \frac{1}{4}(a^2 + b^2 + 2ab\cos 4\beta\cos\phi + (a^2 - b^2)\sin 4\beta) \end{aligned} \tag{B.5}$$

The pump pulses will induce a change in the birefringence, causing a change in A and B. Making use of $\cos(\phi + \Delta\phi) \approx \cos\phi - \Delta\phi\sin\phi$, these changes are:

$$\Delta A = -2ab\cos(4\beta)\Delta\phi\sin\phi \tag{B.6}$$

$$\Delta B = +2ab\cos(4\beta)\Delta\phi\sin\phi \tag{B.7}$$

Finally, the values of θ and $\Delta\theta$ in terms of ϕ and $\Delta\phi$ (making use of the equations derived in appendix A) are:

$$\begin{aligned} \theta &= \frac{1}{2}\cos^{-1}(\frac{A - B}{A + B}) \\ &= \frac{1}{2}\cos^{-1}(\frac{2ab(\cos 4\beta)\cos\phi + (a^2 - b^2)\sin(4\beta)}{a^2 + b^2}) \end{aligned} \tag{B.8}$$

$$\begin{aligned} \Delta\theta &= \frac{(A - B)\Delta A - A(\Delta A - \Delta B)}{(A + B)^2} \\ &= \frac{4ab\Delta\phi\cos(4\beta)\sin\phi}{a^2 + b^2} \end{aligned} \tag{B.9}$$

In conclusion, the $\Delta\theta$ signal we measure varies linearly with the change in birefringence (but may also have contributions from changes in a and b; it is known that dichroism and total transmission depend on temperature, particularly around the phase transition [9]).